



Natural Resources
Canada

Ressources naturelles
Canada

GEOLOGICAL SURVEY OF CANADA
OPEN FILE 8597

**Geothermal assessment of a conventional hydrocarbon
reservoir in eastern Quebec: preliminary field and
petrophysical data**

S. Larmagnat, D. Lavoie, M. M. Rajaobelison, and J. Raymond

2019

Canada The logo of the Government of Canada, featuring a red maple leaf icon.



GEOLOGICAL SURVEY OF CANADA OPEN FILE 8597

Geothermal assessment of a conventional hydrocarbon reservoir in eastern Quebec: preliminary field and petrophysical data

S. Larmagnat¹, D. Lavoie¹, M. M. Rajaobelison², and J. Raymond²

¹Geological Survey of Canada, 490 De la Couronne Street, Quebec, Quebec G1K 9A9

²INRS - ETE, 490 De la Couronne Street, Quebec, Quebec G1K 9A9

2019

© Her Majesty the Queen in Right of Canada, as represented by the Minister of Natural Resources, 2019

Information contained in this publication or product may be reproduced, in part or in whole, and by any means, for personal or public non-commercial purposes, without charge or further permission, unless otherwise specified.

You are asked to:

- exercise due diligence in ensuring the accuracy of the materials reproduced;
- indicate the complete title of the materials reproduced, and the name of the author organization; and
- indicate that the reproduction is a copy of an official work that is published by Natural Resources Canada (NRCan) and that the reproduction has not been produced in affiliation with, or with the endorsement of, NRCan.

Commercial reproduction and distribution is prohibited except with written permission from NRCan. For more information, contact NRCan at nrcan.copyrightdroitdauteur.rncan@canada.ca.

Permanent link: <https://doi.org/10.4095/315028>

This publication is available for free download through GEOSCAN (<https://geoscan.nrcan.gc.ca/>).

Recommended citation

Larmagnat, S., Lavoie, D., Rajaobelison, M. M., and Raymond, J., 2019. Geothermal assessment of a conventional hydrocarbon reservoir in eastern Quebec: preliminary field and petrophysical data; Geological Survey of Canada, Open File 8597, 44 p. <https://doi.org/10.4095/315028>

Publications in this series have not been edited; they are released as submitted by the author.

Table of content

Abstract.....	8
Introduction.....	9
Geological setting	10
Location	12
Methods	13
Fieldwork – visited outcrops.....	13
Val-Brillant and Saint Léon formations siliciclastic lithofacies	14
Sayabec Formation lithofacies	15
Sayabec Formation hydrothermal tectonofacies	16
Probe permeameter (PP)	19
Thermal conductivity and thermal diffusivity.....	20
Results.....	22
Permeability	22
Thermal conductivity and thermal diffusivity.....	24
Porosity and permeability in existing datasets	27
Discussion and conclusion.....	31
Acknowledgements.....	33
References.....	34
Appendix.....	39

List of figures

Figure 1: (A) Stratigraphic section locating the Val-Brillant, Sayabec and Saint-Léon formations. Stratigraphic details are found in Bourque et al. (1995). (B) Simplified geological map of the Témiscouata area in eastern Quebec (Canada) with the location of the Massé No.1 and 2 wells (black star). HTD (yellow arrow) indicates the location of Saint-Cléophas HTD outcrop discussed in text (adopted from Larmagnat et al. (2019b)).....	12
Figure 2: Location map of the study area showing the four tectonostratigraphic zones and outcrops of the Sayabec Fm. Outcrops exposures for reefs and reefs associated facies are indicated by the red stars. Mc is Mont Comi; SC is Saint Charles; LA is Lac Alfred, Red is La Rédemption and Ma is Massé road. The Massé structure correspond to zones 1, 2 and 3. Tectonostratigraphic zones are adopted from Larmagnat et al. (in preparation).....	13
Figure 3: (a) Road cut of Val-Brillant sandstone in the Lac Matapédia sector. (b) Details of the Val-Brillant quartzite made of quartz grains and minor amount of hematite minerals. (c) Contact between the top of the Sayabec Formation and the overlying siltstones of the Saint-Léon Formation. (d) Details of fine-grained siltstone to sandstone with planar parallel and cross-laminations (Saint-Léon Formation).	15
Figure 4: Main carbonate Sayabec facies with (a) nodular limestones, (b) well-bedded bioclastic limestones with (c) centimetric fragments of brachiopod and mollusk shell fragments. (d) Locally, bioclastic limestone from the Sayabec Formation display large (up to 2 cm in diameter) crinoid stems. (e-f) In the western part of the study area, boundstone facies are associated with large stromatoporoids (tens of centimeters large) embedded within a coarse-grained matrix.	16
Figure 5: Hydrothermal alteration in active quarry at La Rédemption village. (a) The hydrothermally altered succession is in contact with unaltered bioclastic facies from the Sayabec Formation (right hand-side of the photograph). (b) Fault plane with well-defined decimeter-long striations. (c) Stratiform dolostone facies corresponding to massively bedded, decimeter-thick layers. (d-e) Close-up views of a highly fractured facies with vugs and fractures filled by saddle dolomite.....	18
Figure 6: (a) Using a gas reservoir (1) and a bike pump (2), permeability measurements are made by applying the probe tip directly on rock surface (3). (b) schematic diagram of the PP-250 device (adapted from Filomena et al. (2014).....	19
Figure 7 : A thermal conductivity scanner (TCS) was used to measure thermal conductivity and thermal diffusivity for both outcrops samples and core samples.....	20
Figure 8: Three main type of orientations used to measure thermal conductivity and thermal diffusivity along rock samples (adapted from Jorand et al. (2013)(a) the scanning line is perpendicular to bedding plane, whereas in (b) and (c) the scanning line is parallel to bedding plane.	21
Figure 9: Ranges of thermal conductivity for the lower Silurian sedimentary succession obtained for the current study, in orange, compared to literature values for common rocks, in green (adapted from Mielke et al. (2017)	26
Figure 10: Permeability vs. porosity for six distinct lithofacies within the Silurian succession in the Témiscouata area. Permeability is here expressed in mD. The dataset covers the Val-Brillant, Sayabec and Saint-Léon formations. The plot combines current results (Tab. 2) and existing data (Tab. 4).....	29
Figure 11: Porosity vs thermal conductivity graph for 6 different lithofacies identified within the Silurian succession in the Témiscouata area. This plot combines current thermal conductivity results (Tab. 3) and existing porosity data (Tab. 4).....	30

Figure 12: Summary of permeability and thermal property ranges obtained for four main types of lithofacies within the lower Silurian rock sequence in the Témiscouata area plotted against threshold values of geothermal potential categories (adopted from Bär et al., 2011).....31

List of tables

Table 1: List of samples collected in the Témiscouata area during the 2018 field campaign. HTD stands for hydrothermal dolomites.....	14
Table 2: Statistics of probe permeametry measurements made on key reservoir facies using outcrop samples. Permeability is measured in milliDarcy (mD). The mean value is then used for the conversion into m ² , with 1mD= 9.86923×10 ⁻¹⁶ m ² . SST stands for sandstone, LST stands for limestone and HTD stands hydrothermal dolomite. N corresponds to the number of rock samples or outcrop exposure used for each lithofacies and n corresponds to the total number of permeability measurements made for each lithofacies.....	23
Table 3: Summary of thermal conductivity and thermal diffusivity values obtained on outcrop samples. SST stands for sandstone, LST stands for limestone and HTD stands for hydrothermal dolomite. Note that N represents the number of samples used in each lithofacies type. Every rock sample was analysed three times for both TC and TD. The volumetric heat capacity was calculated using TC and TD.....	24
Table 4 : Summary of existing data available for the study area. Samples correspond to core samples from wells drilled by Ressources et Énergie Squatex (see Fig. 1) between 2010 and 2015. Permeability and porosity measurements were made at independent labs in Calgary (Alberta), respectively Corelab and AGAT. * HTD stands for Hydrothermal dolomites.	28

Appendix

Appendix 1: Probe permeametry measurements realized directly on outcrop exposures, or on outcrop samples in the laboratory using a Portable Probe Permeameter 250TM from Core Laboratories.....39

Appendix 2: Thermal properties measurements made using a thermal conductivity scanner (TCS) in the Laboratoire ouvert de Géothermie (LOG) at INRS. For each sample, standard used for both conductivity and diffusivity measurements are given.....41

Abstract

In eastern Québec, the Sayabec Formation is a lower Silurian carbonate unit well known for its natural macro porous intervals occurring both at the outcrop scale and in the subsurface, and interpreted as hydrothermal dolomite (HTD) units. The Sayabec Formation represents a potential reservoir analog to the Albion-Scipio oil field (Ordovician, Michigan basin, USA) and has been targeted by a local oil and gas operator since 2010, which resulted in the drilling of about 6000 meters of stratigraphic wells in the Témiscouata area. This provided an ideal case study to test how conventional methods for oil and gas exploration can be applied to assess geothermal properties of reservoir units. To better understand the conventional reservoir properties (e.g. porosity and permeability variability with respect to lithofacies), their spatial heterogeneity and how these properties can be used to evaluate geothermal parameters; outcrops were revisited in the Témiscouata area to collect a consistent, although limited, new sample set of key sedimentary facies within the lower Silurian succession for this pilot project. A total of eight distinctive lithologies were defined and analysed using both an infrared thermal conductivity scanner and probe permeametry, providing critical fine scale assessment of thermophysical properties of the lower Silurian carbonates and clastics. Those preliminary field data are compared with pre-existing porosity and permeability laboratory measurements made on core samples from wells drilled in the same study area.

Introduction

Much of the attention for geothermal energy development has traditionally focused on high temperature geothermal context with the generation of electricity and/or potential exploitation of hot water in deep sedimentary basins (Majorowicz and Grasby, 2010). With low-temperature systems, although electricity generation is feasible with moderate (80°C to 150°C) or even lower (<80°C) temperature, the vast majority of applications relate to heating and cooling buildings using geothermal systems (Raymond and Therrien, 2008; Raymond et al., 2010). In Canada, a number of studies on geothermal potential have been done at the national (e.g. Jessop et al., 1984; Grasby, 2011; Majorowicz and Grasby, 2014; Majorowicz and Minea, 2015a; Raymond et al., 2015; Majorowicz and Grasby, 2019) and the regional scale (Majorowicz and Minea, 2012; 2013; Majorowicz and Minea, 2015b; Bédard et al., 2018) that include studies from northern Québec to southern Québec.

In eastern Québec, the Témiscouata area in the Lower St. Lawrence region (Fig. 1) has been explored over the past ten years for its hydrocarbon reservoir potential in lower Silurian sedimentary units. A significant number of exploration data (well cores and electric logs, field samples) were available for the evaluation of reservoir potential of the lower Silurian Sayabec Formation (Larmagnat et al., 2017; Larmagnat et al., 2019a; Larmagnat et al., 2019b). The availability of this research material, including basic geological and geophysical data, provided a great opportunity to carry out a detailed first appraisal of the geothermal potential of the deep (1500-1700 m depth) lower Silurian units. The area of interest for the geothermal study was part of the regional study of Majorowicz and Minea (2013) who concluded that even though electricity generation is not likely, heat generation could be feasible. More recently, Chabot Bergeron et al. (2016) estimated a corrected temperature ranging between 64-76 °C at a depth of 1889 m (TVD)

based on Harrison et al. (1982) study for the nearby Sun Exploration et al., Mitis No 1 well in the Lac Matapédia area.

The main goal of this research is to demonstrate how data commonly acquired for a conventional hydrocarbon reservoir characterization can be used to evaluate the potential of geothermal energy in a low-temperature environment. To do so, vintage data (local stratigraphy, well electric logs, thermal indicators and bottom temperatures) must be revisited, and a new set of surface and subsurface data must be acquired in order to define key geological attributes (porosity, permeability, thermal conductivity) for the main sedimentary rock types.

The present report compiles preliminary results from fieldwork carried out in 2018 and existing and newly acquired thermal and petrophysical properties (porosity, permeability, thermal conductivity and diffusivity) of key sedimentary rock types in the Massé structure (Fig. 1) in eastern Québec.

Geological setting

The Témiscouata region exposes two main tectonostratigraphic domains (Fig. 1): (1) Cambro-Ordovician tectonostratigraphic units of the Humber (Sainte-Anne River Nappe, Trinité Group, and Dunnage (La Rédemption Complex) zones deformed by the Middle to Late Ordovician Taconian Orogeny and, (2) Upper Ordovician to Lower Devonian strata from the Gaspé Belt (Cabano, Chaleurs, Upper Gaspé Limestones, Fortin/Témiscouata and Gaspé Sandstones groups) that corresponds to post-Taconian foreland basin strata deformed by the Middle Devonian Acadian orogeny (Malo and Bourque, 1993; Bourque et al., 1995; Malo, 2004; Tremblay and Pinet, 2016; Lavoie, 2019).

This study deals with the lower Silurian interval in the Témiscouata area, which consists of the laterally-equivalent Val-Brillant / Robitaille formations overlain by the Sayabec Formation and capped by the late lower to upper Silurian Saint-Léon Formation (Lajoie et al., 1968). The Val-Brillant and Robitaille formations are coeval and laterally equivalent sandstone dominated units. The Val-Brillant Formation is predominantly a well-sorted quartz arenite, whereas the Robitaille Formation consists of a heterogeneous assemblage of mudcracked red mudstone, siltstone and litharenite sandstone, locally containing some quartzarenite beds; both the Val-Brillant and the Robitaille formations are interpreted as nearshore to shoreface deposits (Bourque et al., 1995). The Sayabec Formation is a cyclic carbonate-dominated unit with alternating intervals (members) of outer ramp nodular carbonates and intertidal-subtidal bioclastic to reefal carbonates (Lavoie et al., 1992; Larmagnat et al., 2019a). The alternating intervals result from two episodes of rapid deepening and slow shallowing upward trends. To the east, in the Lac Matapédia area, irregular zones of porous hydrothermal dolostones and breccias are recognized in the Sayabec Formation (Lavoie and Morin, 2004; Lavoie and Chi, 2010); these fractured and porous dolostones have been identified in exploration wells in the Témiscouata area (Larmagnat et al., 2017; Larmagnat et al., 2019a). Finally, the Saint-Léon Formation is composed primarily of green siltstone with subordinate mudstone, sandstone and local conglomerate intervals; the Saint-Léon Formation was deposited in an offshore, most likely pro-delta setting, below fair weather wave-base (Bourque et al., 1995).

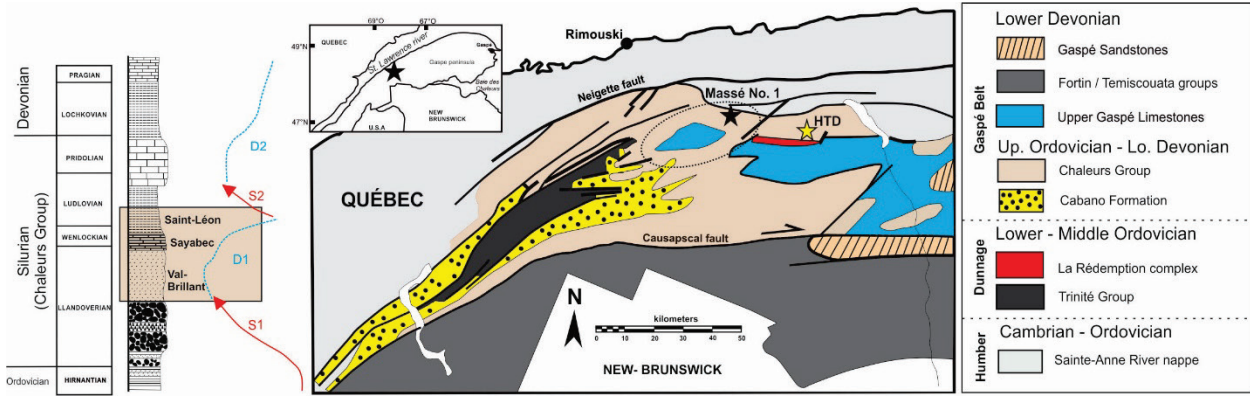


Figure 1: (A) Stratigraphic section locating the Val-Brillant, Sayabec and Saint-Léon formations. Stratigraphic details are found in Bourque et al. (1995). (B) Simplified geological map of the Témiscouata area in eastern Quebec (Canada) with the location of the Massé No. 1 and 2 wells (black star). HTD (yellow star) indicates the location of Saint-Cléophas HTD outcrop discussed in text (adopted from Larmagnat et al. (2019b)). The location of the Massé structure is indicated by the dotted ellipse.

Location

The study area is located between the Lac Matapédia at the NE and the Lac Témiscouata at the SW (Fig. 2), about 30 km southeast of Rimouski. This area belongs to the northern part of the Connecticut Valley-Gaspé synclinorium of the Gaspe Belt. The Taconian unconformity typically separates the Cambro-Ordovician strata to the north and the Ordovician-Devonian strata to the south, but their contact is also faulted in several places (e.g. Lespérance, 1960; Lajoie, 1961; Lajoie et al., 1968). Between 2010 and 2014, the acquisition and/or re-processing of subsurface data (well cores and logs and seismic data; Ressources et Énergie Squatex Inc.) resulted in the recognition of a prospective hydrocarbon play area: the Massé Structure(Figs. 1, 2) Two stratigraphic wells, Massé no. 1 and Massé no.2, were drilled within this structure in 2012 and 2014. The Massé structure is limited by two normal faults and its sedimentary succession was preserved with little deformation, but with local brecciation and/or fractured intervals. The subsurface information was completed by various field campaigns; the last one in 2018 providing new samples and field measurements discussed below.

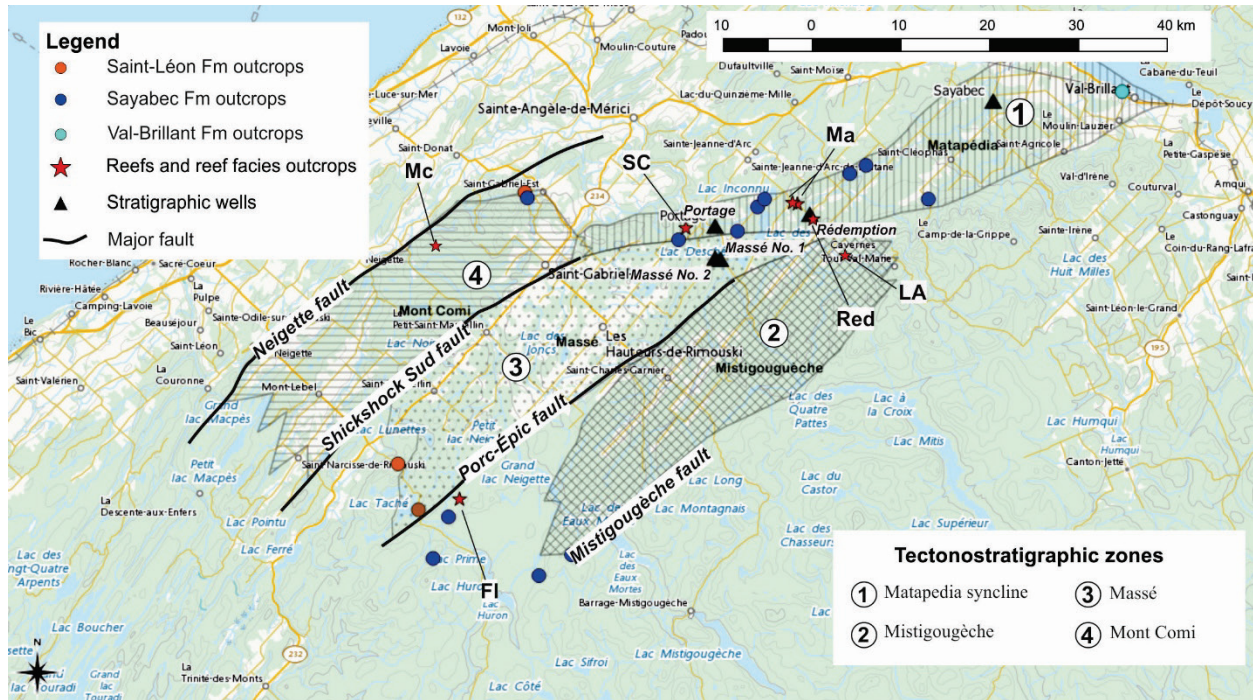


Figure 2: Location map of the study area showing the four tectonostratigraphic zones and outcrops of the Sayabec Fm. Outcrops exposures for reefs and reefs associated facies are indicated by the red stars. Mc is Mont Comi; SC is Saint Charles; LA is Lac Alfred, Red is La Rédemption and Ma is Massé road. The Massé structure correspond to zones 2, 3 and 4. Tectonostratigraphic zones are adopted from Larmagnat et al. (in preparation).

Methods

Fieldwork – visited outcrops

A total of 21 outcrop locations (Fig. 2) were visited and 18 samples collected (Table 1) in the Lower St. Lawrence area, within the 4 tectonostratigraphic zones defined by Larmagnat et al. (2019a).

Stratigraphic Fm	Lithology type	Comments	Location
Saint-Léon	Siltstone	Fine-grained, no structure	Massé
	Siltstone	Fine-grained, with fine scale parallel and cross-laminations	Mont Comi
Sayabec	Sandstone	No alteration	Mont Comi
	Fine-grained limestone	Homogenous, fine-grained mudstone	Rang 3 Massé
Sayabec	Nodular limestone	Bioturbated, with centimetric bioclasts	Mont Comi
	Nodular limestone	-	La Rédemption

Bioclastic limestone	-	St-Cleophas Quarry
Bioclastic limestone	-	La Rédemption Quarry
Reefal debrites	Various centimetric intraclasts (stromatoporoids, crinoids, etc); H ₂ S smell when fractured	Rang 4-5 Massé
Reefal limestone	-	La Rédemption
Reefal limestone	-	ZEC- Lac rouge
Massively bedded HTD	-	St-Cléophas Quarry
HTD breccia	-	St-Cléophas Quarry
HTD breccia	-	St-Cléophas Quarry
HTD breccia	-	La Rédemption Quarry
HTD breccia	-	La Rédemption Quarry
Sandstone	-	Lac Matapédia
<i>Val-Brillant</i>	Sandstone	Lac Matapédia

Table 1: List of samples collected in the Témiscouata area during the 2018 field campaign. HTD stands for hydrothermal dolomites.

Val-Brillant and Saint Léon formations siliciclastic lithofacies

The Val-Brillant Formation is dominated by quartzite with rare calcareous sandstone, siltstone and mudstone. Although some facies indicative of the transition to the Robitaille Formation are noted in this area, the overall facies is strongly reminiscent of the typical Val-Brillant Formation (Fig. 3a-b). The visited outcrops of the Saint-Léon Formation consists of greenish siltstone, mudstone and minor limestones. (Fig. 3c-d).

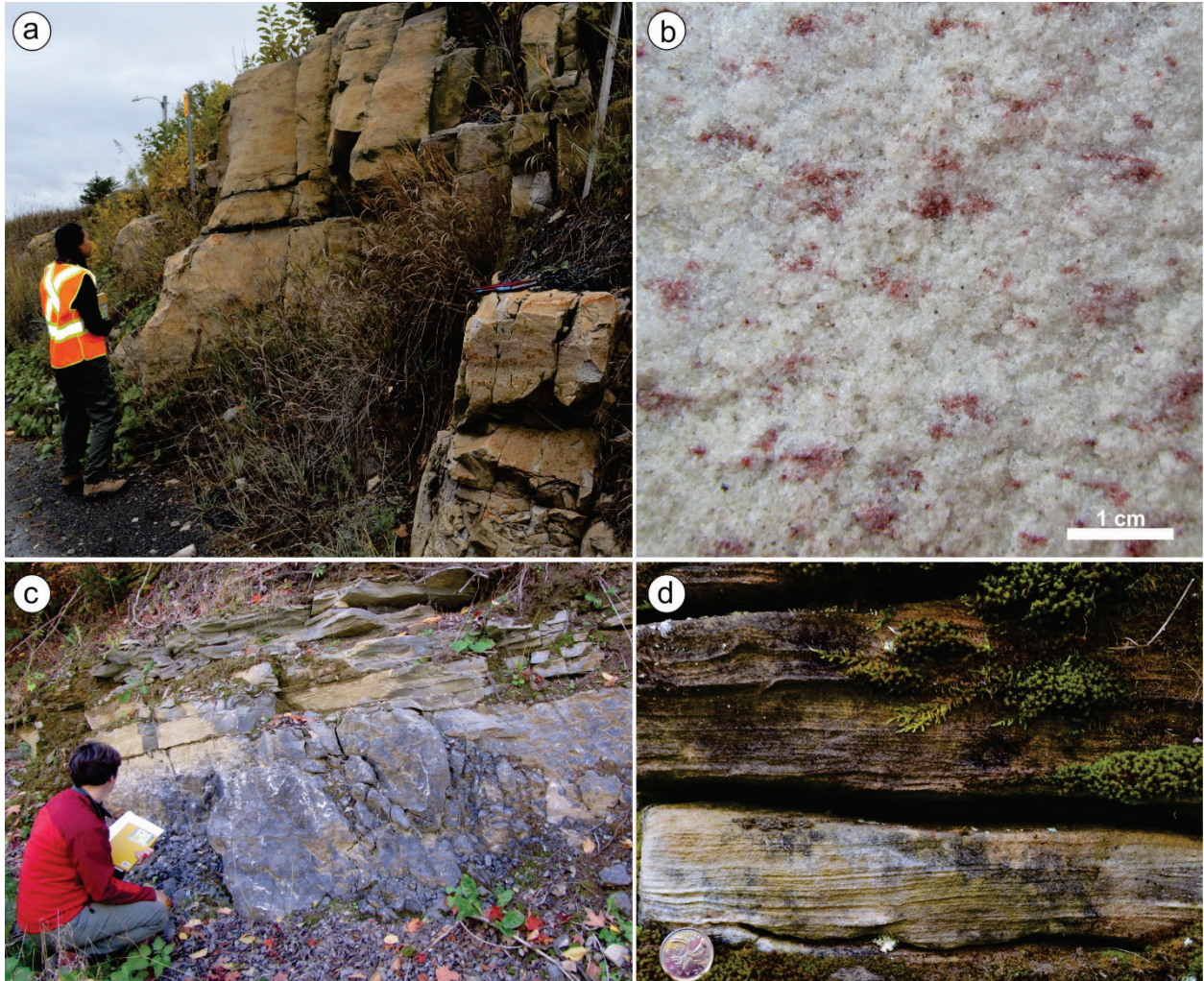


Figure 3: (a) Road cut of Val-Brillant sandstone in the Lac Matapédia sector. (b) Details of the Val-Brillant quartzite made of quartz grains and minor amount of hematite minerals. (c) Contact between the top of the Sayabec Formation and the overlying siltstones of the Saint-Léon Formation. (d) Details of fine-grained siltstone to sandstone with planar parallel and cross-laminations (Saint-Léon Formation).

Sayabec Formation lithofacies

The Sayabec Formation has an average thickness of 300 meters and is dominated by more or less shaly limestone with various bioclastic and reefal limestone units. For the purpose of this work, four main carbonate lithofacies were considered within the Sayabec Formation: (1) fine-grained limestone; (2) nodular (bioturbated) limestone (Fig. 4a); (3) well-bedded bioclastic limestone (Fig. 4b-d) and (4) reefal limestone and reefal debrites (Fig. 4e-f).

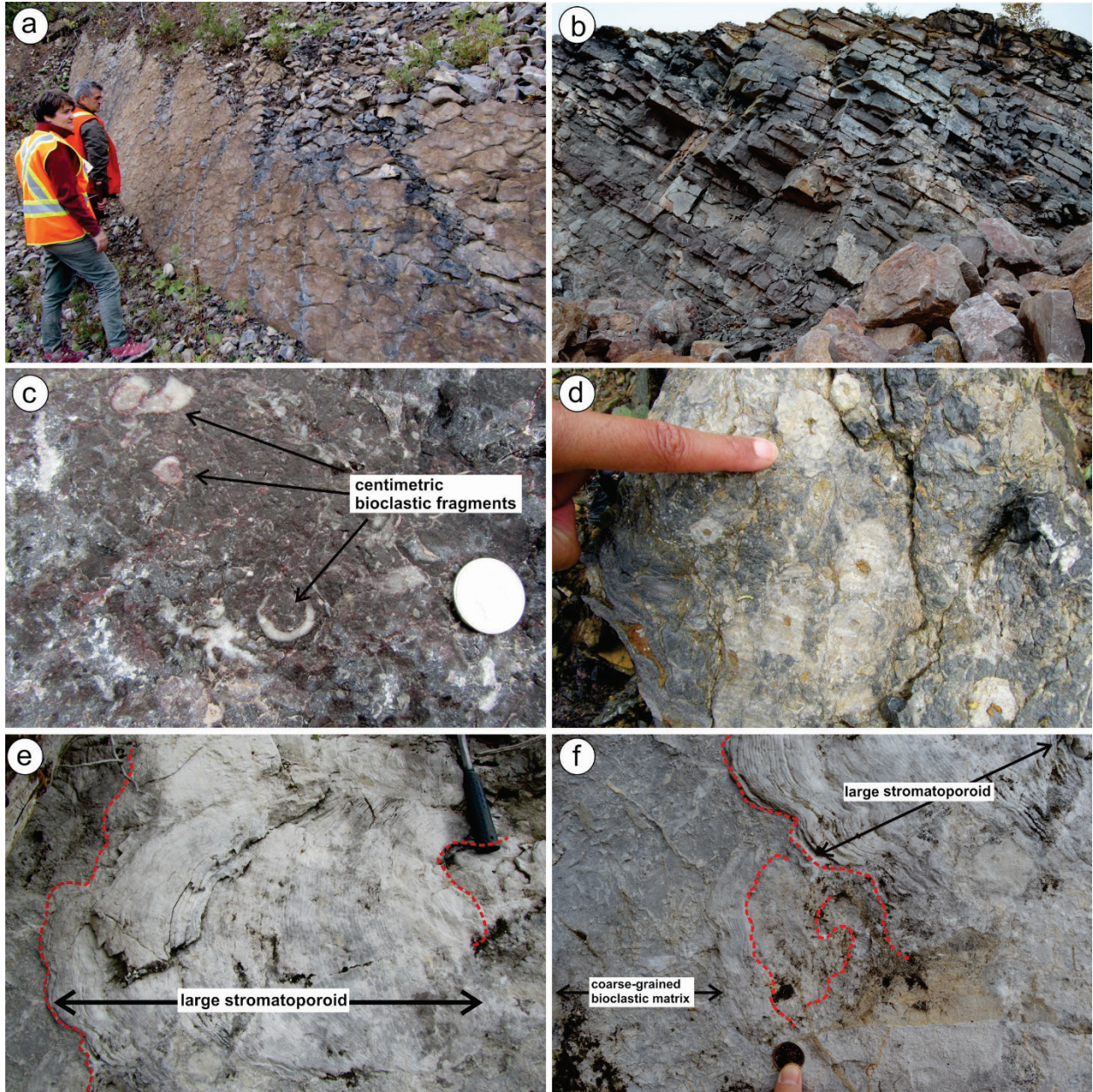


Figure 4: Main carbonate Sayabec facies with (a) nodular limestones, (b) well-bedded bioclastic limestones with (c) centimetric fragments of brachiopod and mollusk shell fragments. (d) Locally, bioclastic limestone from the Sayabec Formation display large (up to 2 cm in diameter) crinoid stems. (e-f) In the western part of the study area, boundstone facies are associated with large stromatoporoids (tens of centimeters large) embedded within a coarse-grained matrix.

Sayabec Formation hydrothermal tectonofacies

Naturally fractured, macro porous intervals, interpreted as hydrothermal in origin (Lavoie and Morin, 2004; Lavoie and Chi, 2010) have been documented at the Saint-Cléophas quarry in the

Lac Matapédia area (Fig 2). During the 2018 field campaign, this locality was revisited and new hydrothermal dolomite outcrops have been discovered in an active quarry near the village of La Rédemption (Fig. 1; Fig. 5a). In the active quarry, dolomitization affected the rock sequence in a large plurimetric zone, both vertically and laterally (Fig. 5a) and the dolomitized/brecciated zones are laterally equivalent and overlain by unaltered bioclastic limestone facies. The dolomitized zones are associated with fractures and faults (N220) with evidence of transpressional movement (slightly inclined, northeast plunging striations; Fig. 5b). Well-bedded dolostone (Fig. 5c) alternate with highly fractured (Fig. 5d) and brecciated zones (Fig. 5e). The reddish dolostone breccia are made of pluricentimetric angular clasts having a jigsaw texture indicative of little displacement; the clasts are set in large crystals of pinkish saddle dolomite (Fig. 5e). From their distinctive petrophysical properties (see below), two dolomite facies are considered: (1) massively-bedded hydrothermal dolomites (HTD) and (2) HTD breccia.

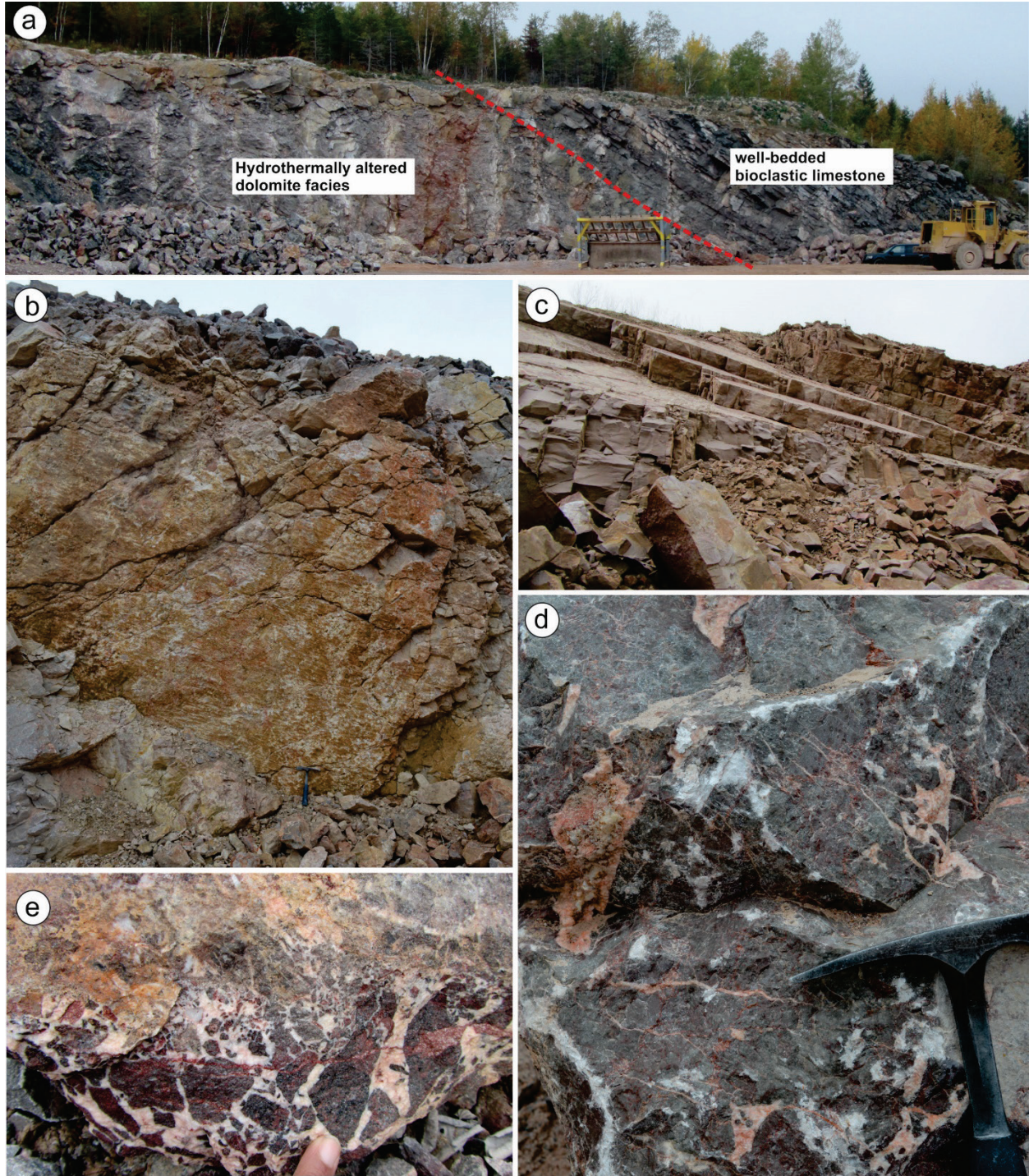


Figure 5: Hydrothermal alteration in active quarry at La Rédemption village. (a) The hydrothermally altered succession is in contact with unaltered bioclastic facies from the Sayabec Formation (right hand-side of the photograph). (b) Fault plane with well-defined decimeter-long striations. (c) Stratiform dolostone facies corresponding to massively bedded, decimeter-thick layers. (d-e) Close-up views of a highly fractured facies with vugs and fractures filled by saddle dolomite.

Probe permeameter (PP)

Permeability of rock units in the field was evaluated using a probe permeameter with measurements made *in situ* using a transient state permeability measurement device. The equipment (Portable Probe Permeameter 250TM from Core Laboratories) takes non-destructive permeability measurements using air supplied to a reservoir with a bike pump (Fig. 6a-b). The probe tip is placed against rock sample faces. Initial flow pressure declines as gas flows into the rock surface, the decay versus time is recorded and the permeability calculated as millidarcy from the pressure (API, 1998). The higher the permeability of the sample, the faster the pressure will decay from an arbitrary initial pressure that was set to 30 psig (pounds per square inch gauge). PP measurements were performed on flat rock or block face and they ended when either the pressure fell below 0.5 psig or the test time exceeded 100 seconds. The PP generates a single permeability measurement for each point.

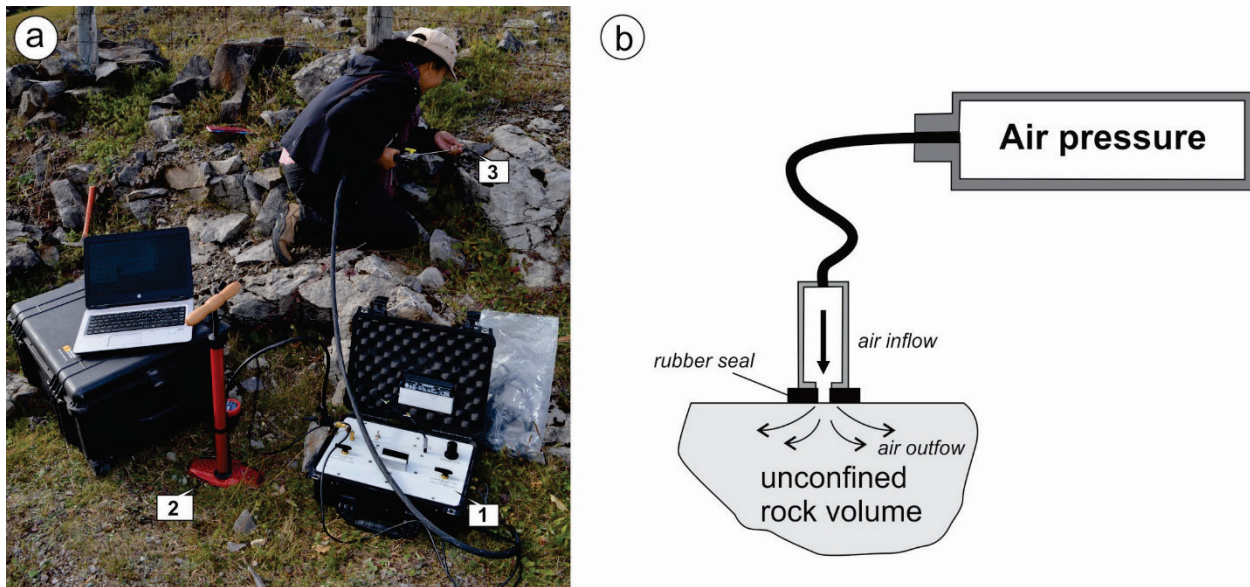


Figure 6: (a) Using a gas reservoir (1) and a bike pump (2), permeability measurements are made by applying the probe tip directly on rock surface (3). (b) schematic diagram of the PP-250 device (adapted from Filomena et al. (2014)).

Thermal conductivity and thermal diffusivity

The thermal conductivity value defines how well the heat is conducted (i.e. transported) by a rock sample, whereas the thermal diffusivity value expresses how fast heat is diffused within that material, i.e. it is a measure of the rate of transfer of heat from a higher to a lower temperature. The thermal diffusivity is a material-specific property describing how quickly a material reacts to a change in temperature. Thermal diffusivity corresponds to the thermal conductivity divided by density and specific heat capacity at constant pressure. A high diffusivity value means that heat transfers rapidly. Thermal properties were estimated using a thermal conductivity scanner (TCS) available at the INRS Laboratoire Ouvert de Géothermie (LOG; Fig. 7). An infrared heat source made by a Lippmann Geophysical Instruments (LGM) is used for transient thermal conductivity (TC) and thermal diffusivity (TD) analysis of hand specimens that are dry and stored at room temperature at least 24h in advance. The instrument uses the optical scanning technique developed by Popov et al. (1999).

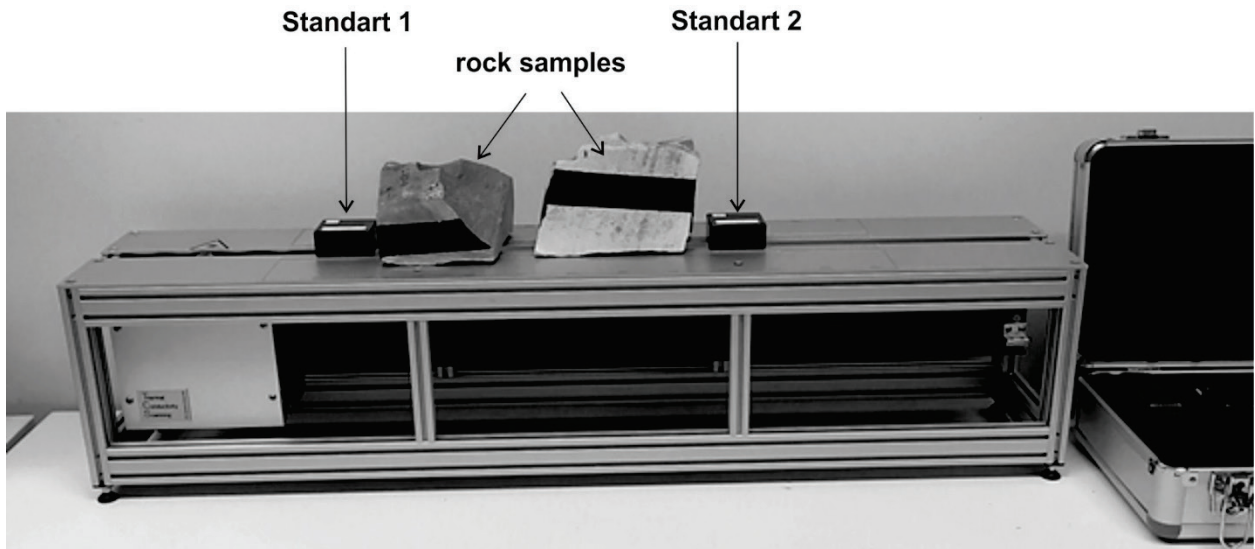


Figure 7 : A thermal conductivity scanner (TCS) was used to measure thermal conductivity and thermal diffusivity for both outcrops samples and core samples.

A moving optical head with an infrared heat source and temperature sensors scan the sample to estimate thermal properties along its length (Jorand et al., 2013). The temperature sensors are located before and after the heat source to measure unperturbed (cold i.e. room temperature) and perturbed (hot) temperature from which the thermal conductivity and diffusivity are inferred according to comparative measurements performed on reference samples placed before and after the rock sample. The orientations of the thermal conductivity and diffusivity measurement are illustrated in Figure 8.

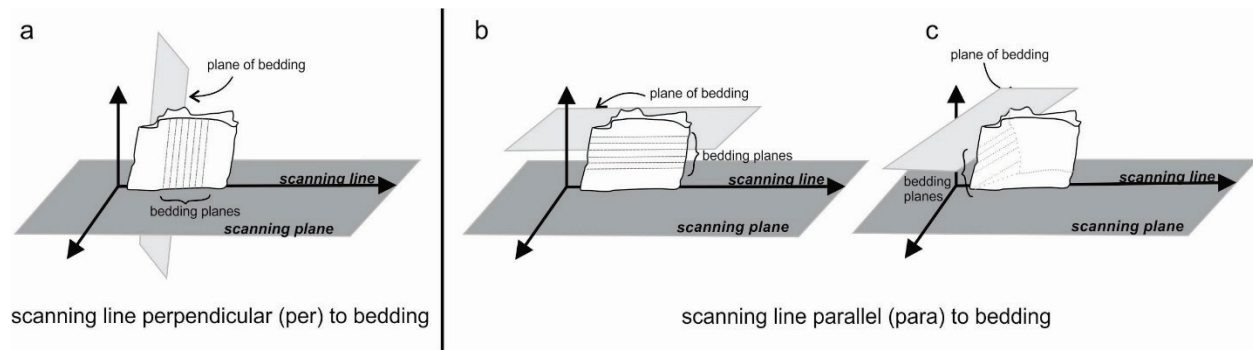


Figure 8: Three main type of orientations used to measure thermal conductivity and thermal diffusivity along rock samples (adapted from Jorand et al. (2013)) (a) the scanning line is perpendicular to bedding plane, whereas in (b) and (c) the scanning line is parallel to bedding plane.

To do these analyses, flat sample faces (from 40 to 500 mm in length) are analyzed along a scan line that have been painted with acrylic black paint to ensure proper infrared absorption to heat the sample. The ranges of measurement of this instrument for thermal conductivity (TC) and diffusivity (TD) are 0.2 to $25 \text{ W m}^{-1} \text{ K}^{-1}$ and 0.6×10^{-6} to $3.0 \times 10^{-6} \text{ m}^2 \text{ s}^{-1}$, with an accuracy of 3 % and 5 %, respectively. Flatness of the sample surface is very important: the spatial irregularity of the sample surface must not exceed $\pm 5 \text{ mm}$. In our case, this was achieved by cutting the rock sample with a diamond-trim saw. The transient heat transfer analysis performed using a thermal conductivity scanner allows a local evaluation of thermal properties along the scan line and the identification of potential heterogeneity. The scanning velocity was set to a median value of

5 mm/s. The factor G used by Popov and collaborators (e.g. Popov et al., 1999; Popov et al., 2016), corresponds to the coefficient of variation (CV). In Popov et al. (2016) another factor, the thermal inhomogeneity factor, F, is defined as the maximum difference in thermal conductivity along the scanning line divided by the average value. According to Albert et al. (2017) high thermal inhomogeneity is defined by $F > 0.35$ and low thermal inhomogeneity by $F < 0.16$. Spatial variations in thermal conductivity along rock sample are most likely due to variability in mineralogical composition, porosity, fracture density, inter-grain contacts and cementation, pore and fracture aspect ratio. Pore aspect ratio is defined as the ratio of pore size to pore throat size, whereas the fracture aspect ratio corresponds to the ratio of fracture length to fracture depth (Liu, 2005). For both TC and TD measurements, all samples were analysed three times and statistical values were averaged. Compared to other techniques for thermal conductivity and thermal diffusivity measurements (*i.e.* divided-bar, and the line source method), optical scanning is particularly useful when used on samples with complex structure and compositions (Popov et al., 1999; Popov et al., 2016), such as hydrothermally altered carbonates.

Results

Permeability

The results of the probe permeability measurements are summarized in Table 2 and the complete data set is provided in Appendix 1. The quality of these measurements is closely related to the efficiency of the seal tightness, as the presence of air leaks will strongly impair/affect the validity of the data (Filomena et al., 2014). The seal efficiency depends on the tightness of the contact between the nozzle, the sealing rubber and the rock sample surface. Those conditions are, however, difficult to control, particularly on outcrops. A poor sealing quality, due to surface roughness for example, can lead to permeability overestimations. Coarse-grained sandstone is a good example

of a very rough surface that may lead to significant overestimations (Filomena et al., 2014). Therefore, permeability values provided in this document should be taken with caution and will be complemented with porosity and permeability values that will be measured with a conventional gas porosimetry (Hassler cells type permeameter) in a future contribution.

Table 2: Statistics of probe permeametry measurements made on key reservoir facies using outcrop samples. Permeability is measured in milliDarcy (mD). The mean value is then used for the conversion into m², with 1mD=9.86923×10⁻¹⁶ m². SST stands for sandstone, LST stands for limestone and HTD stands hydrothermal dolomite. N corresponds to the number of rock samples or outcrop exposure used for each lithofacies and n corresponds to the total number of permeability measurements made for each lithofacies.

	St-Léon Siltstone	Sayabec Fine-grained LST	Sayabec Nodular LST	Sayabec LST Bioclastic	Sayabec Reefal LST	Sayabec Massively bedded HTD	Sayabec HTD breccia	Val-Brillant SST
Permeability (mD)								
Mean	0.95	10.54	11.16	1.24	10.31	10.60	3.95	20.17
Median	0.92	11.80	9.49	1.21	9.81	8.28	3.25	20.17
Range (Max - Min)	1.14	14.90	15.64	1.38	4.30	20.67	7.07	40.14
Min	0.38	0.92	5.76	0.57	8.41	1.43	0.77	0.19
Max	1.52	15.80	19.48	1.94	12.70	22.10	7.84	40.24
Std dev.	0.37	5.76	8.14	0.69	2.67	10.53	3.59	23.34
N	4	1	2	3	2	2	2	1
n	6	5	8	8	9	3	4	5
Mean permeability (m²)	9.50 × 10⁻¹⁷	1.05 × 10⁻¹⁵	1.11 × 10⁻¹⁵	1.24 × 10⁻¹⁶	1.03 × 10⁻¹⁵	1.06 × 10⁻¹⁵	3.95 × 10⁻¹⁶	2.01 × 10⁻¹⁵

Permeability measurements carried out on outcrop samples (Table 1) extend over two orders of magnitude, from 10⁻¹⁵ to 10⁻¹⁷ m². The Saint-Léon siltstone and the Val-Brillant sandstone have respectively the lowest and the highest permeability values. The majority of carbonate facies within the Sayabec Formation are associated with low permeability values (with an average value around 1.10 × 10⁻¹⁵ m²), but the bioclastic limestone and the HTD breccia have even lower permeability values (1.24 × 10⁻¹⁶ and 3.95 × 10⁻¹⁶ m²).

Thermal conductivity and thermal diffusivity

A summary of thermal conductivity and thermal diffusivity measurements carried out on outcrop samples are presented in Table 3 and the complete data set is provided in Appendix 2. Overall, our dataset is consistent with the collections of thermal properties data of sedimentary rocks (at ambient conditions) available in the literature (e.g. Andolfsson, 2013; Mielke et al., 2017). All values obtained fall within the range of 2 to 6 W m⁻¹ K⁻¹ for thermal conductivity (Fig. 8) and within the range of 1 to 2.5 × 10⁻⁶ m² s⁻¹ for thermal diffusivity (Fig. 9).

Table 3: Summary of thermal conductivity and thermal diffusivity values obtained on outcrop samples. SST stands for sandstone, LST stands for limestone and HTD stands for hydrothermal dolomite. Note that N represents the number of samples used in each lithofacies type. Every rock sample was analysed three times for both TC and TD. The volumetric heat capacity was calculated using TC and TD.

Statistics	St-Léon siltstone	Sayabec limestone Fine-grained	Sayabec limestone Nodular	Sayabec limestone Bioclastic	Sayabec limestone Reefal	Sayabec Massively bedded	Sayabec HTD breccia	Val-Brillant sandstone HTD
Thermal Conductivity (W m⁻¹ K⁻¹)								
TC mean								
TC min	3.56	2.66	2.89	3.08	3.05	4.32	3.79	5.31
TC max	3.36	2.28	2.53	2.86	2.76	4.09	3.12	4.34
G (or CV, in %)	3.79	2.95	3.05	3.29	3.27	4.54	4.23	5.88
F (TC _{max} - TC _{min})/TC _{mean} ,	3.75	5.30	4.12	3.18	4.09	3.40	7.50	8.05
Thermal Diffusivity (x10⁻⁶ m² s⁻¹)								
TD mean								
TD min	1.40	1.19	1.31	1.35	1.31	1.69	1.54	4.66
TD max	1.18	0.90	1.10	1.19	1.09	1.37	1.10	2.23
	1.71	1.35	1.64	1.60	1.58	2.29	2.12	27.2

Volumetric heat capacity (MJ m ⁻³ K ⁻¹)	2.54	2.24	2.20	2.28	2.32	2.55	2.46	1.14
N	3	1	1	2	3	1	3	2

More specifically, our dataset for the lower Silurian sedimentary sequence is comparable with the thermal property values available in the thermophysical literature for Paleozoic strata in eastern Canada. The underlying sandstone of the Val-Brillant Formation have the highest thermal conductivity, ranging from 4.34 to 5.88 W m⁻¹ K⁻¹, which is consistent with their high quartz content. However, the Val-Brillant sandstone conductivity values are systematically lower than those of sandstones units of the St. Lawrence Platform, such as the Postdam sandstone, which have thermal conductivity values typically above 6.0 W m⁻¹ K⁻¹ (Raymond et al., 2017). The overlying Saint-Léon siltstones, characterized by a relatively high clay content, have moderate thermal conductivity values, ranging from 3.36 to 3.79 W m⁻¹ K⁻¹. This range of values is consistent with thermal conductivities of similar siltstones in the St. Lawrence Platform (e.g. Queenston Formation).

Within the Sayabec Formation, limestone facies have low to moderate thermal conductivities ranging from 2.28 to 3.29 W m⁻¹ K⁻¹. Four limestone lithofacies were considered (Tab. 3) and although their thermal conductivities are typically around 3 W m⁻¹ K⁻¹, the bioclastic and reefal lithofacies have slightly higher values. The two hydrothermally altered tectonofacies (i.e. breccia and massively bedded dolomites), have higher thermal conductivity values than those of the Sayabec limestones, with values regularly above 4 W m⁻¹ K⁻¹. Furthermore, the dolomite facies of the Sayabec Formation have higher thermal conductivity than those known for the St. Lawrence Platform dolostones, such as the Beauharnois Formation (Raymond et al., 2017).

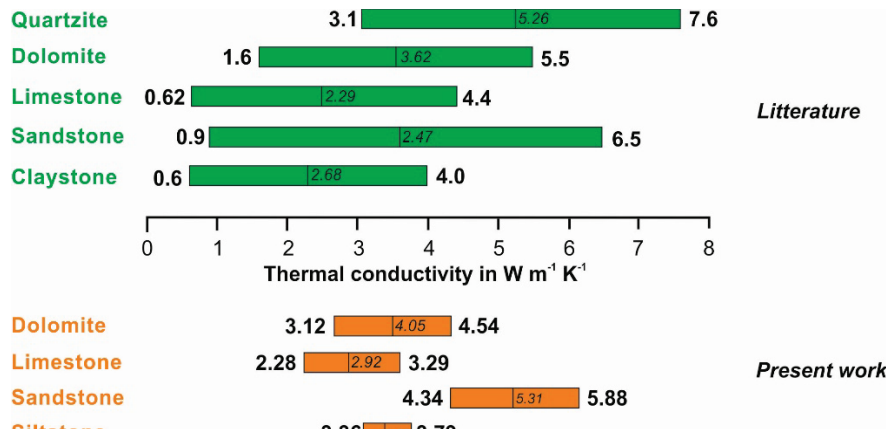


Figure 9: Ranges of thermal conductivity for the lower Silurian sedimentary succession obtained for the current study, in orange, compared to literature values for common rocks, in green. Average values are in italic (adapted from Mielke et al. (2017))

The inhomogeneity factor (F) of a sample was defined as the maximum difference in conductivity along the scanning line divided by the effective thermal conductivity (Popov et al., 1999). It characterizes the variability of its thermal properties in terms of texture, structure and composition, and was determined for every scanning line on every sample. The lower the F factor, the more thermally homogenous the sample is. Saint-Léon siltstone, Sayabec bioclastic and the massively bedded dolomites have low thermal inhomogeneities with $F < 0.16$ (Table 3). The remaining lithofacies all have moderate thermal inhomogeneity (ranging between 0.17 and 0.31) with the Val-Brillant Formation having the highest value (Table 3). As expected, the Sayabec HTD breccias have one of the highest F value (0.29) but still does not exceed the Val-Brillant sandstone value (0.31). In future works, the effect of small-scale variations of rocks properties (such as texture, grain size) on thermal conductivity, will be further studied by measuring inhomogeneity on both dry and water-saturated samples (e.g. Albert et al., 2017). The porosity and fluid saturation have both important control on thermal conductivity and they need to be assessed at the sample scale (Albert et al., 2017).

Thermal diffusivity measurements from our dataset is consistent with existing literature compilations (e.g. Robertson, 1988), since diffusivity of common rocks was found to typically

vary from $7 \times 10^{-7} \text{ m}^2 \text{ s}^{-1}$ (e.g. obsidian), to up to $26 \times 10^{-7} \text{ m}^2 \text{ s}^{-1}$ (e.g. dolomite), although values associated with sandstone can be much higher, with $4.5 \times 10^{-6} \text{ m}^2 \text{ s}^{-1}$ on average (and up to $27 \times 10^{-6} \text{ m}^2 \text{ s}^{-1}$ locally). The volumetric heat capacity is the heat capacity of a rock sample divided by the volume of the sample. It also corresponds to the specific heat capacity (heat capacity per unit of mass; Cp) times the density of the rock (ρ). Using thermal diffusivity and thermal conductivity values, equation (1) was applied to calculate the volumetric specific heat capacity (ρC_p ; expressed in $\text{MJ kg}^{-1} \text{ K}^{-1}$) for each lithofacies:

$$\alpha = \lambda / \rho C_p \quad (1)$$

where α is the thermal diffusivity (TD), λ is the thermal conductivity (TC), ρ is density, and C_p is the specific heat capacity. For the lower Silurian succession, the volumetric heat capacity of carbonate lithofacies varies from 2.20 to 2.32 $\text{MJ K}^{-1} \text{ m}^{-3}$, whereas values measured for dolomite tectonofacies are higher, between 2.46 to 2.55 $\text{MJ K}^{-1} \text{ m}^{-3}$. Overall, our results are similar to ranges of heat capacity values provided by international guidelines such as the Italian UNI11466 (2012) or with literature review by Waples and Waples (2004), except for the Val-Brillant sandstones that have a lower value (1.14 versus $2.05 \text{ MJ m}^{-3} \text{ K}^{-1}$ in Waples and Waples (2004)). More measurements should be done to check if this is due to a sampling artefact, or specific to the Val-Brillant sandstones (e.g. porosity, mineralogy, and particularly the presence of hematite).

Porosity and permeability in existing datasets

In the study area, few petrophysical data ($n=10$) are available for core samples from stratigraphic wells drilled through the Silurian succession (Aubiès-Trouilh, pers. comm. 2016). These data, along with a short description of the samples, are summarized in Table 4.

*Table 4 : Summary of existing data available for the study area. Samples correspond to core samples from wells drilled by Ressources et Énergie Squatex (see Fig. 1) between 2010 and 2015. Permeability and porosity measurements were made at independent labs in Calgary (Alberta), respectively Corelab and AGAT. * HTD stands for Hydrothermal dolomites.*

Stratigraphic unit	Lithology type	Description	Porosity (%)	Permeability (Max) Kair (mD)	Bulk density (kg/m ³)	Grain density (kg/m ³)	Source
<i>Saint-Léon</i>	Calcareous sandstone	Calcareous sandstone (or sandy limestone), with fine-grained sediment and good sorting. Overall well cemented facies	0.7	0.06	2640	2660	Corelab, 2013
	Argillaceous limestone	Fine to medium grained argillaceous limestone with good sorting	0,2	<0,01	2640	2640	Corelab, 2013
	Fine-grained limestone	Fine-grained limestone with horizontal and oblique fractures and veins.	2.1	-	2710	2770	AGAT, 2019
	Fine-grained limestone	Fine-grained, laminated limestone with vertical and oblique fractures and veins.	1.9	-	2740	2790	AGAT, 2019
	Fine-grained limestone	Well sorted fine grained limestone	1,3	0,01	2780	2810	Corelab, 2013
	Bioclastic limestone	Bioclastic limestone with millimetric to plurimillimetric open vugs, often associated with moldic porosity.	3	-	2720	2810	AGAT, 2019
<i>Sayabec</i>	Bioclastic limestone	Fine-grained bioclastic limestone with bioturbations. Small shells (gastropods) are visible.	3,7	0,02	2710	2810	Corelab, 2013
	HTD* breccia	Massive dolomitized limestone with original depositional texture not visible at the macroscale.	4.2	-	2670	2790	AGAT, 2019
	HTD* breccia	Massive dolomitized limestone largely affected by centimetric fractures and dissolution. Original depositional texture is not preserved.	11.3	-	2480	2800	AGAT, 2019
<i>Val-Brillant</i>	Coarse-grained sandstone	Coarse-grained sandstone with good to moderate sorting	20,8	1584	2220	2800	Corelab, 2013

A classic poro-perm coreplot can be made (Fig. 10) when combining the existing dataset (Tab. 4) with the our air permeability values (Tab. 2). The Sayabec limestone facies have low porosity values (between 1.5 to 5%) and relatively low permeabilities (from 0.001 to 10 mD). The overlying

Saint-Léon siltstone and underlying Val-Brillant sandstone are end-members with respectively the lowest and highest porosity and permeability values. The Sayabec HTD dolomite sample lies in between with significantly higher porosity and permeability values than the other Sayabec lithofacies. The amount of data is presently limited ($n=10$), but more data points will be added in future contributions.

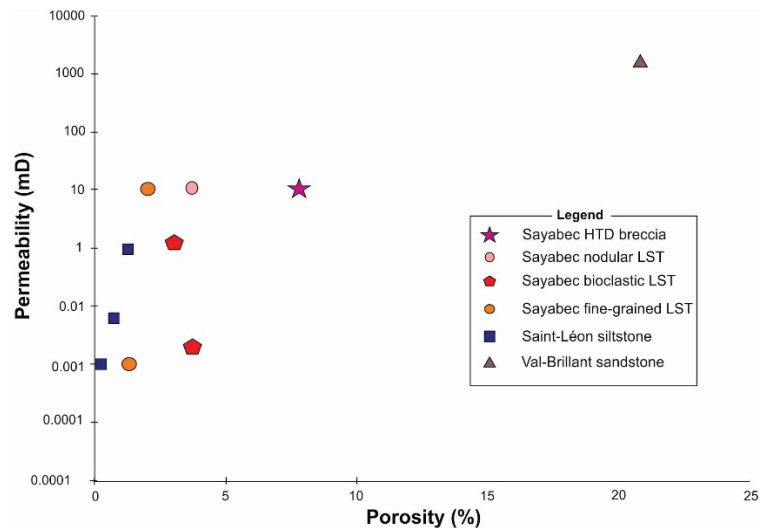


Figure 10: Permeability vs. porosity for six distinct lithofacies within the Silurian succession in the Témiscouata area. Permeability is here expressed in mD. The dataset covers the Val-Brillant, Sayabec and Saint-Léon formations. The plot combines current results (Tab. 2) and existing data (Tab. 4).

Additional correlation was tested, such as the relation between porosity and thermal conductivity (Fig. 11). However, even if R^2 is relatively acceptable and suggest a correlation, the amount of data is also limited ($n=6$), additional data points will have to be added in future contributions to further explore this relationship.

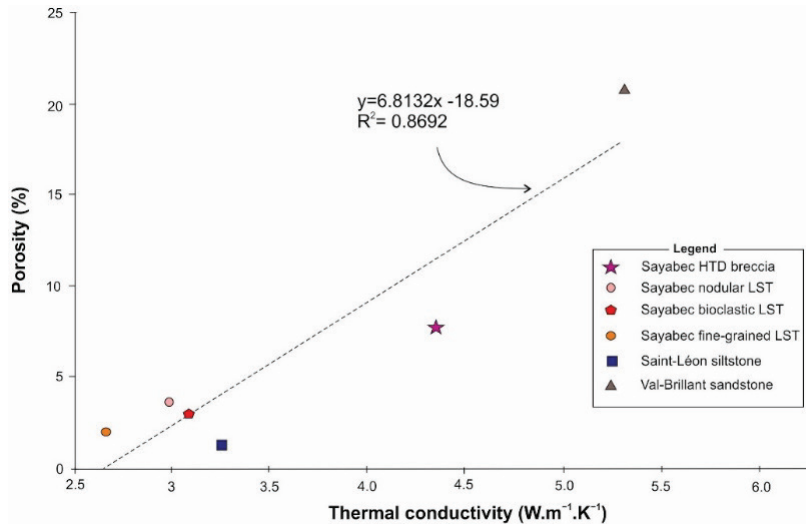


Figure 11: Porosity vs thermal conductivity graph for 6 different lithofacies identified within the Silurian succession in the Témiscouata area. This plot combines current thermal conductivity results (Tab. 3) and existing porosity data (Tab. 4).

Our preliminary results are summarized in Figure 12 to provide a first qualitative assessment of the geothermal properties of four main types of lithofacies from three formations (Saint-Léon, Sayabec and Val-Brillant) within the lower Silurian rock sequence of the Lower St. Lawrence region. This assessment is based on the permeability, thermal conductivity and thermal diffusivity ranges obtained in the present study combined with five geothermal potential categories defined by Bär et al. (2011). All lithofacies have very low permeability values ($< 5 \times 10^{-15} \text{ m}^2$), and low thermal diffusivity values (between 5×10^{-7} and $5 \times 10^{-5} \text{ m}^2/\text{s}$). In terms of thermal conductivities, the overall data suggest medium to very high values with the Val-Brillant Formation sandstone and Sayabec Formation dolomite facies having the highest values of our dataset.

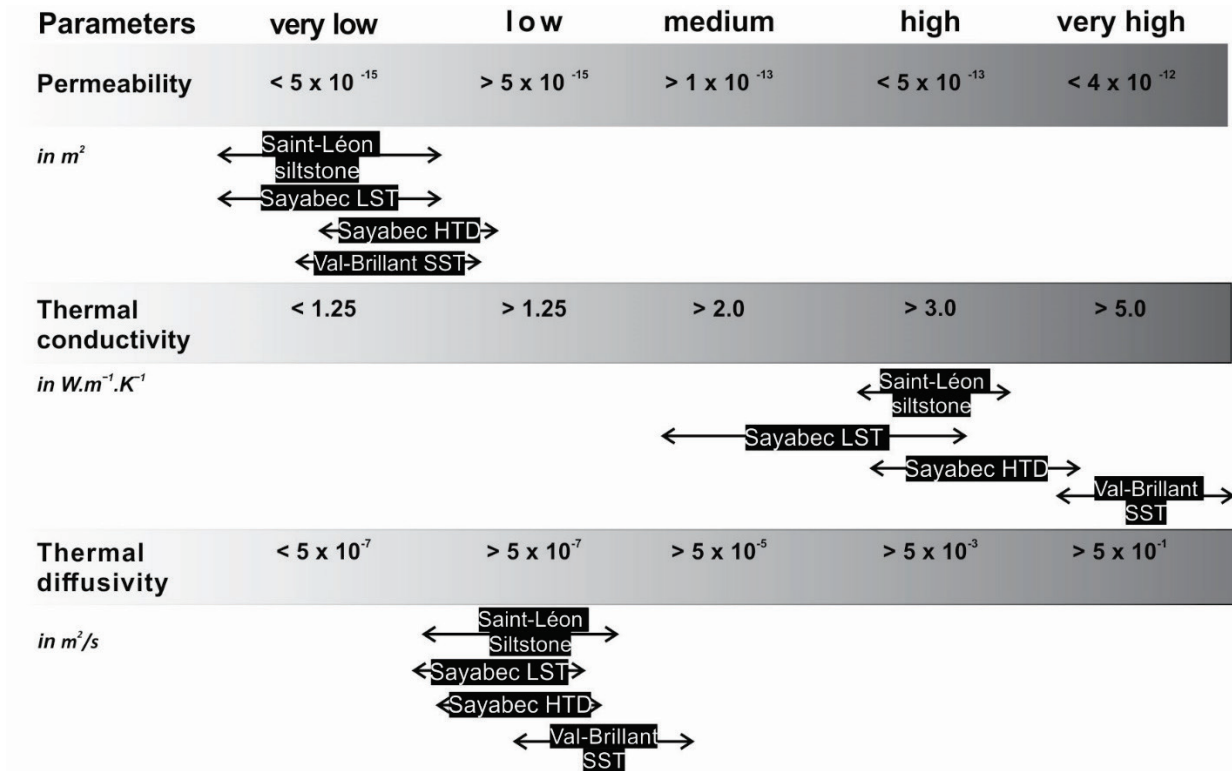


Figure 12: Summary of permeability and thermal property ranges obtained for four main types of lithofacies within the lower Silurian rock sequence in the Témiscouata area plotted against threshold values of geothermal potential categories (adopted from Bär et al., 2011).

Discussion and conclusion

The present work allowed the definition of eight distinctive lithologies from three geological formations based on outcrops (Tab. 2) and core samples (Tab. 3), which were analysed for their thermal properties using an infrared thermal conductivity scanner, whereas petrophysical parameters were obtained with a probe permeameter (for permeability) or from conventional laboratory measurements (for porosity and permeability) in independent laboratories. This preliminary dataset provides critical fine scale information on thermophysical properties of the key lithofacies within the lower Silurian sedimentary succession in the Lower St. Lawrence area.

The Val-Brillant Formation sandstone and the Saint-Léon Formation siltstone provided the highest and lowest values for petrophysical properties (i.e. porosity and permeability values), mainly due

to their mineralogy, being quartz-rich and clay-rich, respectively. These results are in agreement with literature data for typical, siltstone and sandstone.

The four limestone facies of the Sayabec Formation have the lowest mean values of thermal conductivities, with reefal and bioclastic limestones having higher values than the two other lithofacies. The two hydrothermal dolostones tectonofacies have much higher thermal conductivity values that, in some cases, reach values typically associated with sandstones. Also in agreement with the literature (e.g. Brigaud and Vasseur, 1989; Zimmerman, 1989; Popov et al., 2003), our preliminary dataset confirms that thermal conductivity of sedimentary rocks in the lower Silurian succession in eastern Québec is primarily controlled by mineral composition and porosity.

The combination of permeability and thermal conductivity values measured on the same set of samples is key in assessing the potential of geothermal reservoirs (Homuth et al., 2012; Sass and Götz, 2012; Homuth et al., 2015). The concept of thermofacies was first presented by Sass and Götz (2012), who analysed the correlation between geothermal parameters and sedimentary facies for low and mid-enthalpy geothermal systems in central Europe. The definition of thermofacies is crucial to identify heat transfer mechanisms prevailing in geological units. In the Témiscouata area, three specific thermofacies in the Sayabec Formation appear relatively favorable to conductive heat transfer: 1) HTD breccia, 2) massively bedded HTD and 3) reefal bioclastic limestone. They are characterized by high thermal conductivity, but low to very low permeability. As such, they belong to a petrothermal system type (Sass and Götz, 2012; Moeck and Beardsmore, 2014; Moeck, 2014) controlled by conductive heat transfer and would require permeability improvement (e.g. hydraulic fracturing) for an economic reservoir use. The underlying sandstone

in the Val-Brillant Formation, has even higher thermal conductivity values (very high) and also represent a valid candidate for a petrothermal system type.

The study of outcrop analogues bring insights in terms of geometry, structure, fabric and composition of lithofacies (Larmagnat et al., 2017). This is particularly important for heterogeneous macro-porous rocks such as the hydrothermally altered succession, where porosity and structure of pore space have a significant impact on thermal conductivity. In the Sayabec Formation, hydrothermal dolomite intervals are associated with connected macro porosity observed both on outcrops (Lavoie and Morin, 2004) and in the subsurface (Larmagnat et al., 2019b) in the Témiscouata area. A more detailed documentation of the lateral and temporal extension of these intervals, on outcrop exposures, as well as their internal heterogeneity at the macroscale are very important in the perspective of a geothermal potential assessment. This will be addressed in future contributions.

Acknowledgements

The authors would like to thank Ressources et Énergie Squatex Inc., and its geologist A. Aubière-Trouilh, for giving us access to data, as well as for constructive discussions about the present work. We also thank Christine Rivard who kindly accepted to take time to do the internal review of this contribution. The first author was granted a postdoctoral fellowship of the Geological Survey of Canada (Alice Wilson fellowship) with operational funds from the Environmental Geoscience Program of the Lands and Minerals Sector of Natural Resources Canada.

References

- Albert, K., M. Schulze, C. Franz, R. Koenigsdorff and K. Zosseder (2017). "Thermal conductivity estimation model considering the effect of water saturation explaining the heterogeneity of rock thermal conductivity." *Geothermics* 66: 1-12.
- Andolfsson, T. (2013). "Analyses of thermal conductivity from mineral composition and analyses by use of Thermal Conductivity Scanner: a study of thermal properties of Scanian rock types." *Dissertations in Geology at Lund University*.
- API (1998). RP40, Recommended practices for core analysis, 2nd Ed. Washington, DC, American Petroleum Institute.
- Bär, K., D. Arndt, J.-G. Fritsche, A. E. Götz, M. Kracht, A. Hoppe and I. Sass (2011). "3D-Modellierung der tiefengeothermischen Potenziale von Hessen–Eingangsdaten und Potenzialausweisung [3D modelling of the deep geothermal potential of the Federal State of Hesse (Germany)–input data and identification of potential]." *Zeitschrift der Deutschen Gesellschaft für Geowissenschaften* 162(4): 371-388.
- Bédard, K., F.-A. Comeau, J. Raymond, M. Malo and M. Nasr (2018). "Geothermal Characterization of the St. Lawrence Lowlands Sedimentary Basin, Québec, Canada." *Natural Resources Research*: 1-24.
- Bourque, P., D. Brisebois and M. Malo (1995). Gaspé belt. *Geology of the Appalachian–Caledonian Orogen in Canada and Greenland*. Edited by H. Williams. Geological Survey of Canada, *Geology of Canada*. G. S. o. Canada. 6: 316-351.
- Brigaud, F. and G. Vasseur (1989). "Mineralogy, porosity and fluid control on thermal conductivity of sedimentary rocks." *Geophysical Journal International* 98(3): 525-542.
- Chabot Bergeron, A., J. Raymond, M. Malo and F.-A. Comeau (2016). *Évaluation du potentiel de génération d'électricité géothermique en Gaspésie: régions de la vallée de la Matapédia et de Gaspé: Rapport final*, INRS, Centre Eau Terre Environnement.
- Filomena, C., J. Hornung and H. Stollhofen (2014). "Assessing accuracy of gas-driven permeability measurements: a comparative study of diverse Hassler-cell and probe permeameter devices." *Solid Earth* 5(1): 1-11.

Grasby, S. E. (2011). Geothermal energy resource potential of Canada, Natural Resources Canada.

Homuth, S., A. Götz and I. Sass (2012). Facies related thermo-physical characterization of the Upper Jurassic geothermal carbonate reservoirs of the Molasse Basin, Germany. *Geophysical Research Abstracts*.

Homuth, S., A. Götz and I. Sass (2015). "Reservoir characterization of the Upper Jurassic geothermal target formations (Molasse Basin, Germany): role of thermofacies as exploration tool." *Geothermal Energy Science* 3(1): 41-49.

Jessop, A. M., T. J. Lewis, A. S. Judge, A. E. Taylor and M. J. Drury (1984). "Terrestrial heat flow in Canada." *Tectonophysics* 103(1–4): 239-261.

Jorand, R., C. Vogt, G. Marquart and C. Clauser (2013). "Effective thermal conductivity of heterogeneous rocks from laboratory experiments and numerical modeling." *Journal of Geophysical Research: Solid Earth* 118(10): 5225-5235.

Lajoie, J., P. Lespérance and J. Beland (1968). "Silurian Stratigraphy and Paleogeography of Matapedia-Miscouata Region, Quebec." *AAPG Bulletin* 52(4): 615-640.

Lajoie, J. R. (1961). "The origin of the Val Brilliant and Sayabec formations, Quebec."

Larmagnat, S., A. Aubiès-Trouilh, M. Malo and J. Raymond (2017). A conventional play in the Lower St. Lawrence River area (Québec, Canada): the silurian Sayabec Formation. *Geoconvention 2017*. Calgary, Canada.

Larmagnat, S., A. Aubiès-Trouilh, M. Malo; and J. Raymond (2019a). Detailed lithologic log of the lower Silurian Sayabec Formation in the Ressources et Énergie Squatex Massé No 2 well in eastern Québec, Geological Survey of Canada. Open File 8527: 22.

Larmagnat, S., M. Des Roches, L.-F. Daigle, P. Francus, D. Lavoie, J. Raymond, M. Malo and A. Aubiès-Trouilh (2019b). "Continuous sub-millimetric porosity characterization: metric-scale intervals in heterogeneous sedimentary rocks using medical CT scanner." *Marine and Petroleum Geology*.

Lavoie, D. (2019). The Cambrian-Devonian Laurentian Platforms and Foreland Basins in Eastern Canada. *The Sedimentary Basins of the United States and Canada*, Elsevier: 77-128.

Lavoie, D., P.-A. Bourque and Y. Héroux (1992). "Early Silurian carbonate platforms in the Appalachian orogenic belt: the Sayabec–La Vieille formations of the Gaspé–Matapédia basin, Quebec." Canadian Journal of Earth Sciences 29(4): 704-719.

Lavoie, D. and G. Chi (2010). "Lower Paleozoic foreland basins in eastern Canada: tectono-thermal events recorded by faults, fluids and hydrothermal dolomites." Bulletin of Canadian Petroleum Geology 58(1): 17-35.

Lavoie, D. and C. Morin (2004). "Hydrothermal dolomitization in the Lower Silurian Sayabec Formation in northern Gaspé-Matapédia (Québec): Constraint on timing of porosity and regional significance for hydrocarbon reservoirs." Bulletin of Canadian Petroleum Geology 52(3): 256-269.

Lespérance, P. J. (1960). The Silurian and Devonian rocks of the Temiscouata region. Quebec, McGill University. PhD: 264.

Liu, E. (2005). "Effects of fracture aperture and roughness on hydraulic and mechanical properties of rocks: implication of seismic characterization of fractured reservoirs." Journal of Geophysics and Engineering 2(1): 38-47.

Majorowicz, J. and S. E. Grasby (2010). "High potential regions for enhanced geothermal systems in Canada." Natural Resources Research 19(3): 177-188.

Majorowicz, J. and S. E. Grasby (2014). "Geothermal energy for northern Canada: is it economical?" Natural Resources Research 23(1): 159-173.

Majorowicz, J. and S. E. Grasby (2019). "Deep geothermal energy in Canadian sedimentary basins VS. Fossils based energy we try to replace—Exergy [KJ/KG] compared." Renewable Energy 141: 259-277.

Majorowicz, J. and V. Minea (2012). "Geothermal energy potential in the St-Lawrence River area, Québec." Geothermics 43: 25-36.

Majorowicz, J. and V. Minea (2013). "Geothermal anomalies in the Gaspesie Peninsula and the Madeleine Islands, Quebec." GRC Trans 37: 295-300.

Majorowicz, J. and V. Minea (2015a). Geological, Economical and Environmental Assessment of Combined Geothermal Power and Heat Generation in Québec, Canada. World Geothermal Congress Melbourne, Australia.

Majorowicz, J. A. and V. Minea (2015b). "Shallow and deep geothermal energy potential in low heat flow/cold climate environment: northern Québec, Canada, case study." *Environmental Earth Sciences* 74(6): 5233-5244.

Malo, M. (2004). "Paleogeography of the Matapédia basin in the Gaspé Appalachians: initiation of the Gaspé Belt successor basin." *Canadian Journal of Earth Sciences* 41(5): 553-570.

Malo, M. and P.-A. Bourque (1993). "Timing of the deformation events from Late Ordovician to Mid-Devonian in the Gaspé Peninsula." *Geological Society of America Special Papers* 275: 101-122.

Mielke, P., K. Bär and I. Sass (2017). "Determining the relationship of thermal conductivity and compressional wave velocity of common rock types as a basis for reservoir characterization." *Journal of Applied Geophysics* 140: 135-144.

Moeck, I. and G. Beardsmore (2014). A new 'geothermal play type'catalog: Streamlining exploration decision making. Proceedings of the Thirty-Ninth Workshop on Geothermal Reservoir Engineering, Stanford University, Stanford, California.

Moeck, I. S. (2014). "Catalog of geothermal play types based on geologic controls." *Renewable and Sustainable Energy Reviews* 37: 867-882.

Popov, Y., G. Beardsmore, C. Clauser and S. Roy (2016). "ISRM suggested methods for determining thermal properties of rocks from laboratory tests at atmospheric pressure." *Rock Mechanics and Rock Engineering* 49(10): 4179-4207.

Popov, Y., V. Tertychnyi, R. Romushkevich, D. Korobkov and J. Pohl (2003). Interrelations between thermal conductivity and other physical properties of rocks: experimental data. *Thermo-Hydro-Mechanical Coupling in Fractured Rock*, Springer: 1137-1161.

Popov, Y. A., D. F. Pribnow, J. H. Sass, C. F. Williams and H. Burkhardt (1999). "Characterization of rock thermal conductivity by high-resolution optical scanning." *Geothermics* 28(2): 253-276.

Raymond, J., M. Malo, D. Tanguay, S. Grasby and F. Bakhteyar (2015). Direct utilization of geothermal energy from coast to coast: a review of current applications and research in Canada. Proceedings, World Geothermal Congress.

Raymond, J., C. Sirois, M. Nasr and M. Malo (2017). "Evaluating the geothermal heat pump potential from a thermostratigraphic assessment of rock samples in the St. Lawrence Lowlands, Canada." *Environmental Earth Sciences* 76(2): 83.

Raymond, J. and R. Therrien (2008). "Low-temperature geothermal potential of the flooded Gaspé Mines, Québec, Canada." *Geothermics* 37(2): 189-210.

Raymond, J., R. Therrien and L. Gosselin (2010). "Low-temperature geothermal energy in mining environments." *CIM Journal* 1(2): 140-149.

Robertson, E. C. (1988). Thermal properties of rocks, US Geological Survey.

Sass, I. and A. E. Götz (2012). "Geothermal reservoir characterization: a thermofacies concept." *Terra Nova* 24(2): 142-147.

Tremblay, A. and N. Pinet (2016). "Late Neoproterozoic to Permian tectonic evolution of the Quebec Appalachians, Canada." *Earth-Science Reviews* 160: 131-170.

UNI11466 (2012). Sistemi geotermici a pompa di calore - Requisiti per il dimensionamento e la progettazione,

Waples, D. W. and J. S. Waples (2004). "A review and evaluation of specific heat capacities of rocks, minerals, and subsurface fluids. Part 1: Minerals and nonporous rocks." *Natural Resources Research* 13(2): 97-122.

Zimmerman, R. W. (1989). "Thermal conductivity of fluid-saturated rocks." *Journal of petroleum science and engineering* 3(3): 219-227.

Appendix

Appendix 1: Probe permeametry measurements realized directly on outcrop exposures, or on outcrop samples in the laboratory using a Portable Probe Permeameter 250TM from Core Laboratories.

Outcrop or sample number	Lithology	Specifics	Probe Permeametry (PP) in mD	Range		Mean	Median
				Min	Max		
OUT-1-10-2A	Limestone	Tabulate corals with moldic porosity	39.4	19.2	39.4	26.88	23.10
OUT-1-10-2B	Limestone	Micrite	19.2				
OUT-1-10-2C	Sandstone	SST with fresh surface	22				
OUT-1-10-2D	Limestone	Top of limestone unit; altered	45.8	10.7	45.8	26.90	19.50
OUT-1-10-2E	Limestone	15 cm below top of LST unit	24.2				
OUT-1-10-2F	Limestone	75 cm below top of LST unit	10.7				
OUT-2-10-1A	Dolomite	Measurement made parallel to S0	13.4	6.64	19.5	12.44	13.40
OUT-2-10-1B	Dolomite	Measurement made parallel to S0	19.5				
OUT-2-10-1C	Dolomite	Measurement made perpendicular to S0	15.9				
OUT-2-10-1D	Dolomite	Measurement made perpendicular to S0	6.76				
OUT-2-10-1E	Dolomite	Measurement made perpendicular to S0	6.64				
OUT-2-10-2A	Limestone	Measurement made parallel to S0	0.915	0.92	15.8	10.54	11.80
OUT-2-10-2B	Limestone	Measurement made parallel to S0	10.4				
OUT-2-10-2C	Limestone	Measurement made perpendicular to S0	11.8				
OUT-2-10-2D	Limestone	Measurement made parallel to S0	15.8				
OUT-2-10-2E	Limestone	Measurement made perpendicular to S0	13.8				
OUT-2-10-3A	Limestone	Measurement made perpendicular to S0	100	10.5	100	41.03	10.50
OUT-2-10-3B	Limestone	Measurement made perpendicular to S0	12.6				
OUT-2-10-3C	Limestone	Measurement made parallel to S0	7.26	7.11	10.5	8.29	7.26
OUT-2-10-3D	Limestone	Measurement made parallel to S0	7.11				
OUT-2-10-3E	Limestone	Measurement made perpendicular to S0	10.5				
OUT-2-10-5A	Limestone	Measurement made perpendicular to S0	10.6	0.82	10.6	4.55	2.24
OUT-2-10-5B	Limestone	Measurement made perpendicular to S1	2.24				
OUT-2-10-5C	Limestone	Measurement made perpendicular to S2	0.819				
OUT-2-10-5D	Limestone	Measurement made parallel to S0	2.03				
OUT-2-10-5E	Limestone	Measurement made parallel to S0	null				
OUT-2-10-6A	Limestone	Measurement made perpendicular to S0	26	21.6	26	23.80	23.80
OUT-2-10-6D	Limestone	Measurement made perpendicular to S0	21.6				
OUT-2-10-6B	Limestone	Measurement made parallel to S0	12.5	12.5	18.6	15.55	15.55
OUT-2-10-6C	Limestone	Measurement made parallel to S0	18.6				
OUT-2-10-7A	Dolomite	No apparent stratification	null				
OUT-2-10-7B	Dolomite	No apparent stratification	4631				
OUT-2-10-7C	Limestone	No apparent stratification	null				
OUT-3-10-1A	Sandstone	Measurement made parallel to S0	78.3	0.19	78.3	39.24	39.24

OUT-3-10-1B	Sandstone	Measurement made parallel to S0	0.188				
OUT-3-10-1C	Sandstone	Measurement made parallel to S0	null				
OUT-3-10-1D	Sandstone	Measurement made perpendicular to S0	2.17	2.17	2.17	2.17	2.17
OUT-3-10-1E	Sandstone	Measurement made perpendicular to S0	null				
OUT-3-10-8A	Dolomite	No apparent stratification	0.767	0.77	7.84	3.95	4.30
OUT-3-10-8B	Limestone	No apparent stratification	7.84				
OUT-3-10-8C	Dolomite	No apparent stratification	3.25				
OUT-3-10-8B-A	Limestone	Measurement made parallel to S0	1.14	1.54	1.538	1.54	1.54
OUT-3-10-8B-D	Limestone	Measurement made parallel to S0	0.398				
OUT-3-10-8B-B	Limestone	Measurement made perpendicular to S0	0.786	0.63	0.786	0.71	0.71
OUT-3-10-8B-C	Limestone	Measurement made perpendicular to S0	0.625				
OUT-4-10-1A	Limestone	No apparent stratification	0	0	1.05	0.45	0.29
OUT-4-10-1B	Limestone	No apparent stratification	1.05				
OUT-4-10-1C	Limestone	No apparent stratification	0.293				

Appendix 2: Thermal properties measurements made using a thermal conductivity scanner (TCS) in the Laboratoire ouvert de Géothermie (LOG) at INRS. For each sample, standard used for both conductivity and diffusivity measurements are given.

Sample	Lithology	Orientation	Standard	Thermal conductivity					Standard pair	Thermal Diffusivity		
				TCmean	TCmin	TCmax	G (%)	F		TDmean	TDmin	TDmax
<i>OUT-1-10-I</i>	Siltstone/ SST	parallel	TC (Ref) = 2.390	4.21	3.91	4.39	2.06	0.11	TD(Ref1)= 0.850 and TD(Ref2)= 2.760	1.539	1.236	2.136
		parallel		4.15	3.99	4.36	2.47	0.09		1.464	1.224	1.729
		parallel		4.10	3.91	4.27	2.00	0.09		1.525	1.287	1.837
		parallel	Average	4.15	3.94	4.34	2.18	0.10		1.51	1.25	1.90
<i>OUT-1-10-I</i>	Siltstone/ SST	parallel	TC (Ref) = 2.390	4.04	3.80	4.46	4.30	0.17	TD(Ref1)= 0.850 and TD(Ref2)= 2.760	1.511	1.243	2.062
		parallel		3.97	3.73	4.27	3.59	0.14		1.447	1.268	1.747
		parallel		3.95	3.70	4.23	3.41	0.14		1.462	1.329	1.617
		parallel	Average	3.99	3.74	4.32	3.77	0.15		1.47	1.28	1.81
<i>OUT-1-10-2C</i>	St Leon Siltstone/ SST	parallel	TC (Ref) = 2.390	3.37	3.19	3.51	1.69	0.10	TD(Ref1)= 0.850 and TD(Ref2)= 2.760	1.576	1.154	2.168
		parallel		3.40	3.22	3.55	1.62	0.10		1.431	1.13	1.714
		parallel		3.44	3.24	3.62	2.26	0.11		1.413	1.179	1.922
		parallel	Average	3.40	3.21	3.56	1.86	0.10		1.47	1.15	1.93
<i>OUT-1-10-2D</i>	St Leon Siltstone/ SST	parallel	TC (Ref) = 2.390	3.10	2.98	3.25	1.96	0.09	TD(Ref1)= 0.850 and TD(Ref2)= 2.760	1.225	1.085	1.372
		parallel		3.12	3.04	3.21	1.38	0.06		1.255	1.133	1.355
		parallel		3.09	2.99	3.18	14.34	0.06		1.253	1.102	1.389
		parallel	Average	3.10	3.00	3.21	5.89	0.07		1.24	1.11	1.37
<i>OUT-1-10-2D</i>	St Leon Siltstone/ SST	perpend.	TC (Ref) = 2.390	3.20	2.94	3.59	5.20	0.20	TD(Ref1)= 0.850 and TD(Ref2)= 2.760	1.307	1.093	1.583
		perpend.		3.16	2.86	3.43	5.02	0.18		1.351	1.124	1.591
		perpend.		3.17	2.96	3.51	5.01	0.17		1.285	1.103	1.484
		perpend.	Average	3.18	2.92	3.51	5.08	0.19		1.31	1.11	1.55
<i>OUT-2-10-2</i>	Sayabec Fine-grained LST	parallel	TC (Ref) = 2.390	2.66	2.26	2.98	5.74	0.27	TD(Ref1)= 0.850 and TD(Ref2)= 2.760	1.189	0.883	1.375
		parallel		2.66	2.29	2.94	5.20	0.25		1.197	0.937	1.377
		parallel		2.67	2.29	2.93	4.94	0.24		1.178	0.882	1.311
		parallel	Average	2.66	2.28	2.95	5.30	0.25		1.19	0.90	1.35
<i>OUT-2-10-5</i>	Sayabec nodular LST	perpend.	TC (Ref) = 2.390	2.88	2.66	3.01	3.08	0.12	TD(Ref1)= 0.850 and TD(Ref2)= 2.760	1.355	1.172	1.606
		perpend.		2.87	2.65	3.04	3.02	0.14		1.374	1.168	1.906
		perpend.		2.91	2.70	3.05	2.82	0.12		1.361	1.135	1.675
		perpend.	Average	2.89	2.67	3.03	2.97	0.13		1.36	1.16	1.73
<i>OUT-2-10-5</i>	Sayabec nodular LST	parallel	TC (Ref) = 2.390	2.86	2.38	3.04	2.94	0.23	TD(Ref1)= 0.850 and TD(Ref2)= 2.760	1.249	1.029	1.567
		parallel		2.88	2.40	3.05	2.91	0.23		1.268	1.046	1.57
		parallel		2.91	2.41	3.10	2.94	0.24		1.266	1.054	1.519
		parallel	Average	2.88	2.40	3.06	2.93	0.23		1.26	1.04	1.55

<i>OUT-2-10-7C</i>	Sayabec bioclastic LST	parallel	<i>TC (Ref) = 2.390</i>	3.13	2.95	3.22	1.71	0.09	<i>TD(Ref1)= 0.850 and TD(Ref2)= 2.760</i>	1.383	1.22	1.643	
		parallel		3.15	3.05	3.29	1.51	0.08		1.375	1.189	1.662	
		parallel		3.12	3.03	3.22	1.43	0.06		1.324	1.167	1.482	
		parallel	<i>Average</i>	3.14	3.01	3.25	1.55	0.08	<i>Average</i>	1.36	1.19	1.60	
<i>OUT-2-10-7C</i>	Sayabec bioclastic LST	parallel	<i>TC (Ref) = 2.390</i>	3.04	2.76	3.28	4.00	0.17	<i>TD(Ref1)= 0.850 and TD(Ref2)= 2.760</i>	1.447	1.22	1.815	
		parallel		3.04	2.84	3.26	3.91	0.14		1.43	1.213	1.607	
		parallel		3.05	2.84	3.26	3.33	0.14		1.345	1.168	1.559	
		parallel	<i>Average</i>	3.04	2.81	3.27	3.75	0.15	<i>Average</i>	1.41	1.20	1.66	
<i>OUT-3-10-8B</i>	Sayabec bioclastic LST	parallel	<i>TC (Ref) = 2.390</i>	2.96	2.59	3.22	4.92	0.21	<i>TD(Ref1)= 0.850 and TD(Ref2)= 2.760</i>	1.301	0.935	1.949	
		parallel		2.96	2.64	3.23	4.87	0.20		1.346	0.952	1.848	
		parallel		2.96	2.63	3.30	5.44	0.23		1.261	1.782	0.942	
		parallel	<i>Average</i>	2.96	2.62	3.25	5.08	0.21	<i>Average</i>	1.30	1.22	1.58	
<i>OUT-3-10-8B</i>	Sayabec bioclastic LST	parallel	<i>TC (Ref) = 2.390</i>	3.18	3.01	3.41	2.43	0.13	<i>TD(Ref1)= 0.850 and TD(Ref2)= 2.760</i>	1.393	1.149	1.718	
		parallel		3.22	2.98	3.36	2.03	0.12		1.35	1.179	1.532	
		parallel		3.20	3.04	3.40	2.55	0.11		1.285	1.15	1.437	
		parallel	<i>Average</i>	3.20	3.01	3.39	2.33	0.12	<i>Average</i>	1.34	1.16	1.56	
<i>OUT-2-10-3</i>	Sayabec reefal debrites	parallel	<i>TC (Ref) = 2.390</i>	3.09	3.00	3.19	1.46	0.06	<i>TD(Ref1)= 0.850 and TD(Ref2)= 2.760</i>	1.343	1.093	1.629	
		parallel		3.09	2.97	3.21	1.46	0.08		1.283	1.078	1.609	
		parallel		3.09	2.99	3.18	1.23	0.06		1.277	1.108	1.441	
		parallel	<i>Average</i>	3.09	2.99	3.19	1.38	0.07	<i>Average</i>	1.30	1.09	1.56	
<i>OUT-2-10-3</i>	Sayabec reefal debrites	perpend.	<i>TC (Ref) = 2.390</i>	3.11	2.96	3.19	1.91	0.07	<i>TD(Ref1)= 0.850 and TD(Ref2)= 2.760</i>	1.368	1.186	1.575	
		perpend.		3.13	2.96	3.24	1.97	0.09		1.326	1.104	2.411	
		perpend.		3.13	2.96	3.27	2.55	0.10		1.301	1.135	1.552	
		perpend.			3.12	2.96	3.24	2.14	0.09	<i>Average</i>	1.33	1.14	1.85
<i>OUT-2-10-6</i>	Sayabec Reefal LST	parallel	<i>TC (Ref) = 2.390</i>	3.02	2.38	3.37	9.18	0.33	<i>TD(Ref1)= 0.850 and TD(Ref2)= 2.760</i>	1.345	0.957	1.909	
		parallel		3.05	2.39	3.43	9.42	0.34		1.29	0.922	2.134	
		parallel		3.05	2.38	3.44	9.39	0.35		1.241	0.899	1.744	
		parallel	<i>Average</i>	3.04	2.38	3.41	9.33	0.34	<i>Average</i>	1.29	0.93	1.93	
<i>OUT-4-10-1</i>	Sayabec Reefal LST	parallel	<i>TC (Ref) = 2.390</i>	3.23	2.96	3.42	3.09	0.14	<i>TD(Ref1)= 0.850 and TD(Ref2)= 2.760</i>	1.331	0.937	1.726	
		parallel		3.24	2.93	3.40	3.04	0.15		1.32	1.104	1.621	
		parallel		3.21	2.88	3.46	3.24	0.18		1.299	1.074	1.537	
		parallel	<i>Average</i>	3.22	2.92	3.43	3.13	0.16	<i>Average</i>	1.32	1.04	1.63	
<i>OUT-2-10-7B</i>	Sayabec HTD breccia	perpend.	<i>TC (Ref) = 2.390</i>	3.67	2.48	4.41	14.20	0.53	<i>TD(Ref1)= 0.850 and TD(Ref2)= 2.760</i>	1.564	0.834	2.44	
		perpend.		3.69	2.48	4.34	14.18	0.50		1.47	0.827	1.845	
		perpend.		3.68	2.43	4.31	14.02	0.51		1.501	0.791	2.425	
		perpend.	<i>Average</i>	3.68	2.46	4.35	14.13	0.51	<i>Average</i>	1.51	0.82	2.24	

<i>OUT-2-10-7B</i>	Sayabec HTD breccia	parallel	<i>TC (Ref) = 2.390</i>	3.92	3.01	4.46	11.29	0.37	<i>TD(Ref1)= 0.850 and TD(Ref2)= 2.760</i>	1.74	1.309	2.144
		parallel		3.87	2.95	4.42	11.08	0.38		1.894	1.293	2.522
		parallel		3.89	3.05	4.41	10.68	0.35		2.016	1.549	3.034
		parallel	<i>Average</i>	3.90	3.00	4.43	11.02	0.37	<i>Average</i>	1.88	1.38	2.57
<i>OUT-3-10-8A</i>	Sayabec HTD breccia	parallel	<i>TC (Ref) = 2.390</i>	3.19	2.98	3.35	2.72	0.12	<i>TD(Ref1)= 0.850 and TD(Ref2)= 2.760</i>	1.286	1.129	1.468
		parallel		3.17	3.04	3.33	2.18	0.09		1.282	1.15	1.448
		parallel		3.10	2.90	3.61	2.49	0.23		1.318	1.171	1.508
		parallel	<i>Average</i>	3.15	2.97	3.43	2.47	0.15	<i>Average</i>	1.30	1.15	1.47
<i>OUT-3-10-8A</i>	Sayabec HTD breccia	parallel	<i>TC (Ref) = 2.390</i>	3.08	2.90	3.52	5.57	0.20	<i>TD(Ref1)= 0.850 and TD(Ref2)= 2.760</i>	1.183	1.035	1.38
		parallel		3.07	2.89	3.58	5.71	0.22		1.189	0.989	1.401
		parallel		3.10	2.94	3.61	5.57	0.22		1.144	0.976	1.366
		parallel	<i>Average</i>	3.08	2.91	3.57	5.62	0.21	<i>Average</i>	1.17	1.00	1.38
<i>OUT-3-10-8C</i>	Sayabec HTD breccia	parallel	<i>TC (Ref) = 2.390</i>	4.58	3.52	4.97	6.50	0.32	<i>TD(Ref1)= 0.850 and TD(Ref2)= 2.760</i>	1.706	1.062	3.07
		parallel		4.61	3.41	5.08	7.38	0.36		1.828	1.004	2.675
		parallel		4.73	3.54	5.22	7.97	0.36		1.622	1.027	2.072
		parallel	<i>Average</i>	4.64	3.49	5.09	7.28	0.35	<i>Average</i>	1.72	1.03	2.61
<i>OUT-3-10-8C</i>	Sayabec HTD breccia	parallel	<i>TC(Ref) = 6.35</i>	4.26	3.85	4.59	4.69	0.17	<i>TD(Ref1)= 0.850 and TD(Ref2)= 2.760</i>	1.701	1.291	2.435
		parallel		4.24	3.82	4.57	4.53	0.18		1.596	1.124	2.255
		parallel		4.26	3.85	4.56	4.26	0.17		1.609	1.192	2.745
		parallel	<i>Average</i>	4.25	3.84	4.57	4.49	0.17	<i>Average</i>	1.64	1.20	2.48
<i>OUT-2-10-7A</i>	Sayabec massive\ly bedded HTD	parallel	<i>TC (Ref) = 2.390</i>	4.38	4.20	4.54	7.97	0.08	<i>TD(Ref1)= 0.850 and TD(Ref2)= 2.760</i>	1.856	1.417	2.662
		parallel		4.32	4.01	4.62	3.06	0.14		1.818	1.441	2.681
		parallel		4.35	4.10	4.62	2.21	0.12		1.719	1.374	2.422
		parallel	<i>Average</i>	4.35	4.10	4.59	4.41	0.11	<i>Average</i>	1.80	1.41	2.59
<i>OUT-2-10-7A</i>	Sayabec massive\ly bedded HTD	perpend.	<i>TC (Ref) = 2.390</i>	4.31	4.04	4.62	3.02	0.14	<i>TD(Ref1)= 0.850 and TD(Ref2)= 2.760</i>	1.673	1.279	2.331
		perpend.		4.27	4.11	4.47	2.30	0.08		1.503	1.317	1.726
		perpend.		4.26	4.07	4.38	1.82	0.07		1.56	1.363	1.92
		perpend.	<i>Average</i>	4.28	4.07	4.49	2.38	0.10	<i>Average</i>	1.58	1.32	1.99
<i>OUT-3-10-1A</i>	Val Brilliant SST	parallel	<i>TC (Ref) = 2.390</i>	4.72	1.87	5.75	23.08	0.82	<i>TD(Ref1)= 0.850 and TD(Ref2)= 2.760</i>	5.503	2.138	68.101
		parallel		4.87	1.91	6.06	23.44	0.85		3.936	1.935	15.605
		parallel		4.81	1.88	5.93	23.42	0.84		null	null	null
		parallel	<i>Average</i>	4.80	1.88	5.91	23.31	0.84	<i>Average</i>	4.72	2.04	41.85
<i>OUT-3-10-1A</i>	Val Brilliant SST	parallel	<i>TC (Ref) = 2.390</i>	5.41	5.05	5.79	2.75	0.14	<i>TD(Ref1)= 0.850 and TD(Ref2)= 2.760</i>	2.934	1.945	6.654
		parallel		5.48	5.20	5.82	2.75	0.11		3.305	1.993	7.923
		parallel		5.40	5.08	5.79	3.09	0.13		2.913	2.128	7.889
		parallel	<i>Average</i>	5.43	5.11	5.80	2.86	0.13	<i>Average</i>	3.05	2.02	7.49

<i>OUT-3-10-IB</i>	Val Brilliant SST	perpend.	<i>TC (Ref) = 2.390</i>	5.31	5.07	5.65	2.66	0.11	<i>TD(Ref1)= 0.850 and TD(Ref2)= 2.760</i>	8.955	2.666	86.09 9
		perpend.		5.57	5.19	6.06	3.48	0.16		3.495	2.106	10.53 6
		perpend.		5.52	5.12	5.98	4.04	0.16		6.138	2.056	40.13 4
		perpend.	<i>Average</i>	5.46	5.13	5.90	3.39	0.14	<i>Average</i>	6.20	2.28	45.59
<i>OUT-3-10-IB</i>	Val Brilliant SST	parallel	<i>TC (Ref) = 2.390</i>	5.58	5.26	5.99	3.07	0.13	<i>TD(Ref1)= 0.850 and TD(Ref2)= 2.760</i>	7.269	2.449	32.60 9
		parallel		5.55	5.23	5.90	2.52	0.12		3.097	2.53	4.443
		parallel		5.50	5.21	5.87	2.34	0.12		3.462	2.766	5.36
		parallel	<i>Average</i>	5.54	5.23	5.92	2.64	0.12	<i>Average</i>	4.61	2.58	14.14